Physics Essentials of Particle Therapy

Dennis Mah, Michael Moyers, Ken Kang-Hsin Wang,
Eric Diffenderfer, John Cuaron, and Mark Pankuch

Contents

D. Mah (✉)
ProCure New Jersey, Somerset, NJ, USA
e-mail: dennis.mah@nj.procure.com

M. Moyers
Shanghai Proton and Heavy Ion Center, Shanghai, China
e-mail: Michael.F.Moyers@sphic.org.cn

K. Kang-Hsin Wang
Johns Hopkins Hospital, Baltimore, MD, USA
e-mail: kwang27@jhmi.edu

E. Diffenderfer
University of Pennsylvania, Philadelphia, PA, USA
e-mail: Eric.Diffenderfer@uphs.upenn.edu

J. Cuaron
Memorial Sloan Kettering Cancer Center, New York City, NY, USA
e-mail: cuaronj@mskcc.org

M. Pankuch
Northwestern Medicine, Chicago Proton Center, Warrenville, IL, USA
e-mail: mark.pankuch@nm.org

1.1   History of Light Ion Teletherapy

1.1.1   Rationale for Light Ion Beam Teletherapy

- There are three reasons for using light ion beams for teletherapy: (1) the low entrance dose and almost zero dose delivered distal to the target results in the ratio of nontarget tissue dose to target dose being smaller than with other radiation beams; (2) with appropriate collimation, the dose gradients at the lateral and distal sides of the targets are higher than with other radiation beams thereby offering higher dose gradients between the target and normal tissues; (3) for ions heavier than helium, the increase in RBE with increasing depth results in the target receiving a higher RBE dose than the tissues on the entrance side.
- Light ions are a subset of heavy charged particles and are defined as ions with atomic numbers less than 20 [1–3]. Although six different ions have been used for human treatments, the majority of patients have been treated with protons, helium ions, and carbon ions. Figure 1.1 shows the approximate number of patients treated with different heavy charged particle beams between 1954, when
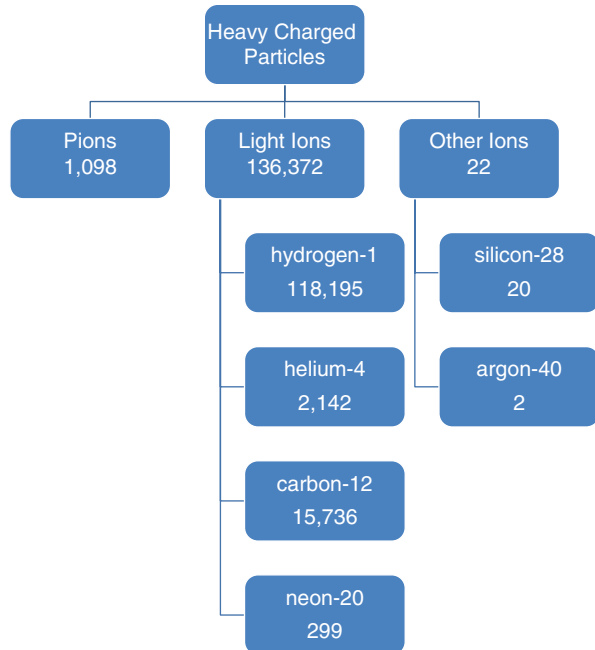

Fig. 1.1 Approximate number of patients treated with different heavy charged particle beams from 1954 to 2015. Figure adapted from Vatnitsky and Moyers [4] and updated with data from Jermann [5] to reflect recent data

treatments commenced, through 2015. Table 1.1 is a list of major milestones since the first patient was treated with a proton beam in 1954.

- As of 2015, there were approximately 50 facilities in the world treating patients with light ion beams. Figure 1.2 plots the number of operating facilities according to continent.

Table 1.1 Major milestones in light ion teletherapy according to year and location

Year	Location	Milestone
1954	Berkeley	First patient treated with protons
1957	Uppsala	First patient treated with uniform scanning with protons
1958	Berkeley	First patient treated with helium ions
1965	Boston	First AVM treated with protons
1975	Boston	First ocular melanoma treated with protons
1977	Berkeley	First patients treated with carbon and neon ions
1979	Chiba	First patients treated with modulated scanning with protons
1989	Tsukuba	First proton patients treated with respiratory beam gating
1990	Loma Linda	First patient treated in hospital with protons
1991	Loma Linda	First use of rotating gantry for proton beams
1996	Loma Linda	First electronic x-ray imaging with computerized analysis for daily alignment of proton beams
1997	Darmstadt	First patients treated with modulated scanning with carbon ions
1998	Loma Linda	100 patients treated with protons in 1 day at a single facility
2005	Loma Linda	173 patients treated with protons in 1 day at a single facility
2012	Heidelberg	First use of rotating gantry for carbon ion beams

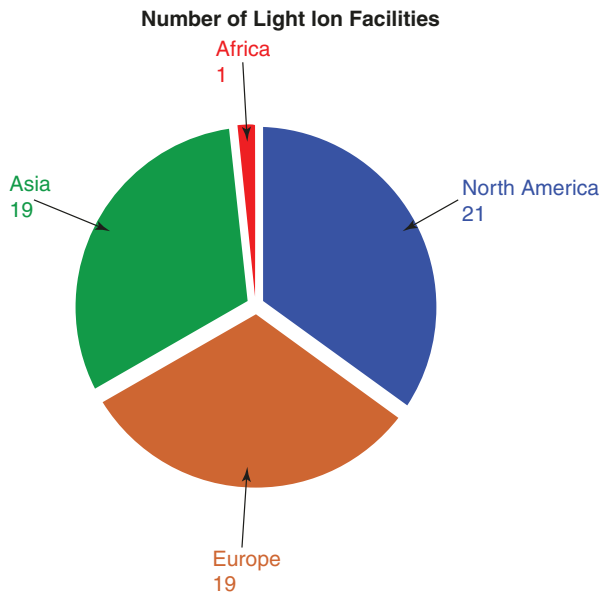Table from Vatnitsky and Moyers [4] and used with permission from Medical Physics Publishing

Number of Light Ion Facilities

Fig. 1.2 Number of light ion facilities operating worldwide as of 2015 according to continent. Data compiled from Jermann [5]

1.2   Basic Physics

- Like electrons, protons interact with material through ionization and Coulomb scattering, but because protons are 1836 times heavier than electrons, they are not deflected much by scattering with electrons. With a much lower probability, protons can interact with the nucleus resulting in lateral deflections and an increasing lateral spreading of the beam at depth [6].
- The maximum energy of protons used to treat patients is typically between 220 and 250 MeV. The velocity of protons having these energies is about 0.6 times the speed of light. As protons slow down, they spend more time passing by molecules thus causing more ionization resulting in a larger dose deposition toward the end of their range. The shape of the most distal region is called the Bragg peak (Fig. 1.3a). To treat finite size targets in depth, beams of multiple energies may be combined to generate a spread out Bragg peak (SOBP). Proton range depends on the beam energy with higher-energy beams being more penetrating. Proton range is typically defined as the depth of the 90% isodose on the distal edge of the Bragg peak (Fig. 1.3b). The modulation width is typically defined as the width of the SOBP between the depth of the proximal 90% dose and the depth of the distal 90% dose.

1.2.1   Penumbra

- Lateral penumbra may be defined as in photon beams, i.e., the distance between the 80 and 20% dose levels. The lateral penumbra width increases with increasing depth. The 90–50% penumbra width is about ~3% of the depth for double
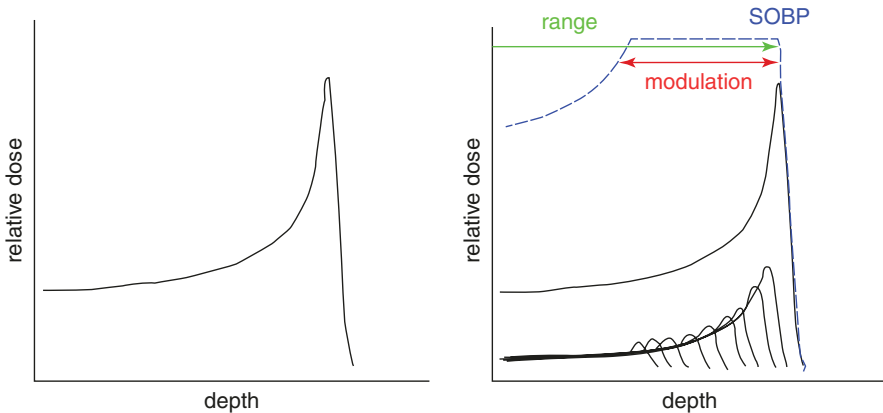

Fig. 1.3 (**a**) Pristine (monoenergetic) energy proton beam depth dose distribution in water. (**b**) A weighted average of the depth dose distributions in water from several energy proton beams results in a spread out Bragg peak. The modulation width is characterized by the difference between the depths of the 90% isodose at the proximal and distal ends of the SOBP
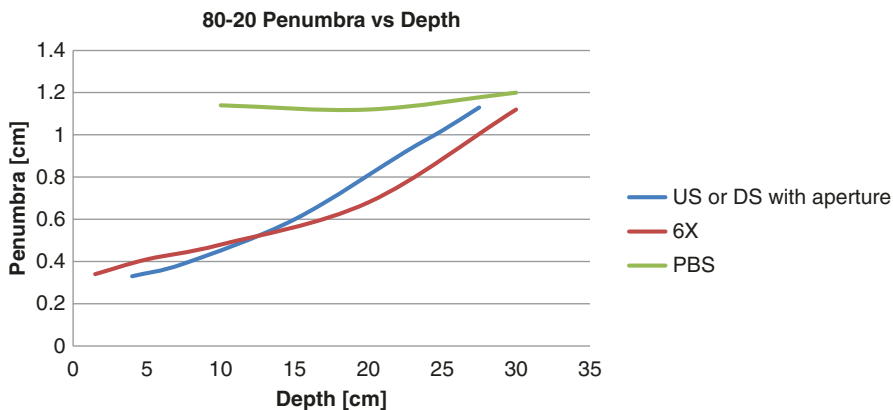
80-20 Penumbra vs Depth

Fig. 1.4 Comparison of lateral penumbra for proton double-scattered beam with aperture, proton pencil beam scanning without collimation, and collimated 6 MV x-rays in water. The 6 MV x-ray data were taken from [8]. The proton data were generated for an IBA universal nozzle using a Raystation treatment planning system. The results are meant to show the trend, and results will vary between centers due to differences in the delivery systems (e.g., nozzle design)

scattering systems [7]. Figure 1.4 compares lateral penumbra for a collimated proton beam, collimated 6 MV x-ray beam, and proton pencil beam scanning without collimation. In general, the penumbra for pencil beam scanning (PBS) is constant with depth. The penumbra for PBS delivered beams can be improved by an aperture [9, 10].

- The distal penumbra results primarily from range straggling (which is ~1.2% of the range) and from beam energy spread (which depends upon the proton source) [11].
- Ions heavier than protons, such as carbon ions, have both sharper lateral and distal penumbra because their larger mass results in less scatter. While in theory, carbon could have a penumbra 1/3 that of protons, scanning with such a small spot would result in unacceptable delivery times. Consequently, spots larger than the minimum possible are used. However, it is the RBE (see below) effects that make these particles heavier than protons more compelling.

1.2.2   In Patient

- Tissue inhomogeneity issues are much worse in protons than photons, but protons also have dose homogeneity advantages over photons and fewer proton fields are often used. Patients have inhomogeneities in terms of composition and density. Scatter increases with atomic number. Changes in density alter the range in a manner that is difficult to fully account for using CT-based planning (see range uncertainty). Interfaces between different materials can lead to in and out scatter resulting in hot or cold spots at the interfaces. These effects are not fully calculated in pencil beam-based treatment planning systems but can be modeled

using Monte Carlo [12]. Additionally, not only the range, but also the shape and distal penumbra of the SOBP can be affected by inhomogeneities; in many cases, the slope of the distal penumbra is enlarged by inhomogeneities.

1.3   Relative Biological Effectiveness (RBE)

- In radiation therapy, much of the clinical experience has been gained through photon treatments, which is based on the physics parameter dose, not directly related to the biological end points, such as tumor control probability (TCP) or normal tissue complication probability (NTCP) [13, 14]. Biological endpoints for an identical physical dose can be different for proton and photon therapy, *i.e.*, equal doses of photon and proton therapy do not produce the same clinical or biological outcomes.
- To take advantage of the clinical experience gained from the photon therapy and account for the difference of the biological effect between the two modalities, proton prescriptions are based on a factor (relative biological effectiveness, RBE) times the physical proton dose.
- The RBE for proton therapy (or another particle therapy) can be defined as—given the same biological effect—the ratio of the physical doses between the reference beam, *e.g.*, photon, and the proton beam.

$$RBE = \frac{Dose_{reference}\left(Biological\,effect\right)}{Dose_{proton}\left(Biological\,effect\right)}$$

- From the available in vitro and in vivo data, recent publications [13, 14] have suggested that RBE is a function of:
  - *Dose*: From clonogenic cell survival curve (cell survival fraction *versus* dose, Fig. 1.5), within the low dose region, protons typically show a less pronounced shoulder compared to photons, which implies larger α/β (α is the parameter describing the cell killing per Gy of the initial linear component and β describes the killing per Gy^2 of the quadratic component of the linear-quadratic survival curve). It renders that for a given survival fraction, the ratio between photon and proton dose (RBE) can be different at low dose region than that of the high dose region (Fig. 1.5).
  - *Tissue type:* Recent findings from clonogenic cell survival data [14] has suggested that the RBE increases with decreasing $(\alpha/\beta)_x$ {α_x and β_x are the dose response parameters in the linear-quadratic model in photon therapy}, although large uncertainties existed in these data. This finding suggests that proton treatments can potentially induce larger RBEs for late responding normal tissues than for tumor tissue with high $(\alpha/\beta)_x$ values.
  - *Proton beam properties (linear energy transfer, LET):* Given the energy of clinical proton beams, in general, RBE increases with increasing LET. The LET is

Fig. 1.5 Schematic cell survival curves for photon radiation (*solid*) and proton radiation (*dashed*)
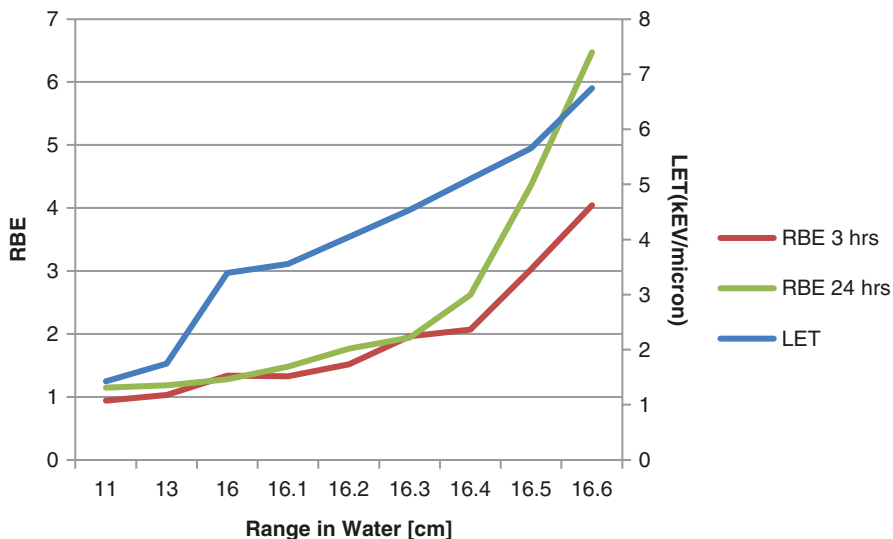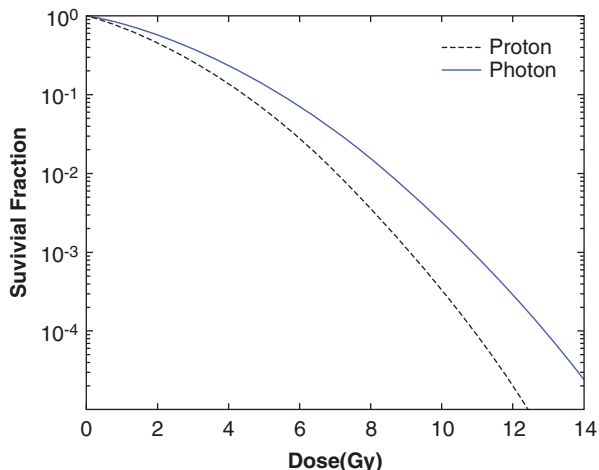

Fig. 1.6 LET and RBE as a function of depth along the distal edge of a proton beam

also a function of depth in a proton beam, which results in an increase of RBE with depth. This effect can be demonstrated using Monte Carlo simulation of LET of a 152 MeV proton beam, plotted alongside RBE values of the same beam using DNA double strand breaks as a biological endpoint (Fig. 1.6) [15].

– The increase of RBE also increases the effective range of the RBE-weighted depth dose, which can result in an effective 1–3 mm shift of the depth of the distal penumbra region. It is also important to keep in mind that the LET values depend on the treatment field, particularly the SOBP modulation width.

- Clinical (generic) RBE value: Although proton RBE depends on the above mentioned factors and considerable uncertainties in RBE values remain, the use of a constant RBE of 1.1, recommended by ICRU 78 report [16], does not seem unreasonable if an average value of is desired cross the proton ranges used clinically. To follow the same convention given in the ICRU report,

$$D_{RBE} = 1.1 \times D,$$

where D is the proton absorbed dose in Gy and D_{RBE} in Gy is the RBE-weighted proton absorbed dose equivalent to the dose of photons that would produce the same clinical outcome as a proton dose D. For example, one prescribes the proton absorbed dose to the target as $D = 63$ Gy, and the RBE-weighted dose can be expressed as $63 \times 1.1 \rightarrow D_{RBE} = 70$ Gy(RBE). In other words, to deliver a photon equivalent dose 70 Gy(RBE) to a target, one would deliver a proton dose of 63 Gy.

1.3.1   Terminology

1. *RBE-weighted dose* is a biologically weighted quantity used to define a dose of protons that would produce an identical biological effect as a dose of photons. Due to the consistent characteristics of the cobalt-60 beam and the undetectable biological differences between typical photon beams and Co-60 beams, all photon fields are referenced to a cobalt-60 equivalent dose. This has led to commonly used terminology such as "cobalt equivalent," "gray equivalent" or "cobalt-gray equivalent" with units such as Gy(E), GyE, and CGE to describe an RBE-weighted absorbed dose. These are not the standard SI unit but are still used. As mentioned above, ICRU [16] recommended to report the RBE-weighted dose in DRBE [in units of Gy(RBE)].

   It is common practice to incorporate the doses in the treatment planning system in RBE-weighted dose so that clinicians can evaluate in terms of equivalent doses rather than physical doses.
   - Clinic considerations: Because proton RBE is a function of dose, tissue type, and LET, the following points potentially affect clinic outcome [13].
     - *Dose effect*: Because RBE depends on dose, the RBE can be potentially reduced, less than 1.1, with increasing dose, especially for hypofractionated cases.
     - *Tissue type*: Tumors with low $(\alpha/\beta)_x$ values, such as prostate tumors, might show a RBE higher than 1.1. In contrast, tumors with very high $(\alpha/\beta)_x$ values could have lower RBE.
     - *The RBE increases with depth* and recent data suggests that RBE values are significantly higher than previously estimated, especially at the distal edge (24). During planning, one should be cautious if aiming a beam toward an organ at risk (OAR) even if it is behind the target, because the combination

of the high-LET/RBE region at the distal falloff region and range uncertainties can potentially result in an undesirable radiobiological dose to the downstream OAR.

- *Delivery modalities*: Investigators recently indicate [17] LET variation appears to be potentially significant in IMPT delivery, such as distal edge tracking (DET)-IMPT where the DET-IMPT plans resulted in considerably increased LET values (increased RBE) in critical structures. In contrast, the 3-D IMPT shows more favorable LET distributions than does DET-IMPT. It is important to be aware of the LET variation for different delivery techniques.
- Considering these uncertainties, it is crucial that physicians, treatment planners, and physicists work together to mitigate, track, and report acute and long-term toxicities and outcomes among patients treated with proton therapy. Clinical data will help to determine whether these uncertainties should guide refinement of treatment planning and delivery, or alternatively, can be safely disregarded.

1.3.2 Ions Heavier than Protons

- Heavier charged particles (such as argon, neon, silicon, and carbon ions) and fast neutrons are considered high-LET radiation. Currently, carbon ions are the most often used high-LET therapy worldwide because of a number of potential advantages over photon and proton therapy in both physical and biological aspects [18, 19];
  - *Dose distribution*: Both the lateral and distal penumbras are narrow. The energy spread and range straggling of the particles are smaller for carbon ions. The dose ratio between the SOBP and entrance plateau is higher than protons. Nuclear fragmentation after the distal end of the Bragg peak can be a potential disadvantage when using carbon. However, this aspect is usually minimal because the dose is low and the fragments are lower-LET particles.
  - *Therapeutic gain*: The LET in a clinical ion beam increases with depth, leading to the increase of RBE. Among the heavier ions, carbon ions have the advantage of the highest peak-to-plateau RBE ratio. At the position of the SOBP, where the target regions are located, high-LET radiation makes ion beams specifically effective for the treatment of some tumor types that are resistant to low-LET radiation. These features open the potential to treat tumors that are deeply located and resistant to proton or photon treatment. Other advantages for carbon ions include reducing the oxygen enhancement ratio (OER), radiosensitivity of the cell cycle dependency, and suppressing the repair of radiation damage.
- The RBE of SOBP carbon beam exhibits substantially greater variation with depth than that of a proton beam, being dependent upon the position within the SOBP, dose, dose per fraction, and tissue type. For the same depth and tissue, the RBE at the center of the SOBP can vary between three and five, and the ratio between target and skin doses may vary by a factor of two [18, 19].

- Treatment planning: Since large RBE variations are seen for carbon ion therapy, unlike proton therapy, a single value is not sufficient to accurately/safely describe the biological effective dose. For treatment planning, RBE values must be estimated as accurately as possible. Two different strategies and modeling approaches were chosen by two leading carbon facilities, the National Institute of Radiological Sciences (NIRS) in Japan and Gesellschaft für Schwerionenforschung (GSI) in Germany, respectively.
  - NIRS employed an experimentally oriented approach [3]. It is based on the measurements of RBE in vitro, which are used to determine the shape of the biological effective depth dose profile. The clinical RBE value is then determined by establishing equivalency between carbon and neutron beams to make use of the experience in neutron therapy. The NIRS group found a carbon beam which possesses a dose averaged LET of 80 keV/µm results in an equivalent biological response to those from the neutron beams. The clinical RBE was defined as 3, the same as that used in neutron therapy at the point where the dose averaged LET value is 80 keV/µm. Figure 1.7 shows the physical dose distribution required in the SOBP to yield a constant biological response (dose) across the SOBP. To further obtain the clinical/prescribed dose, the biological dose at every depth is multiplied by the ratio of the biological and clinical RBEs at the neutron equivalent position.
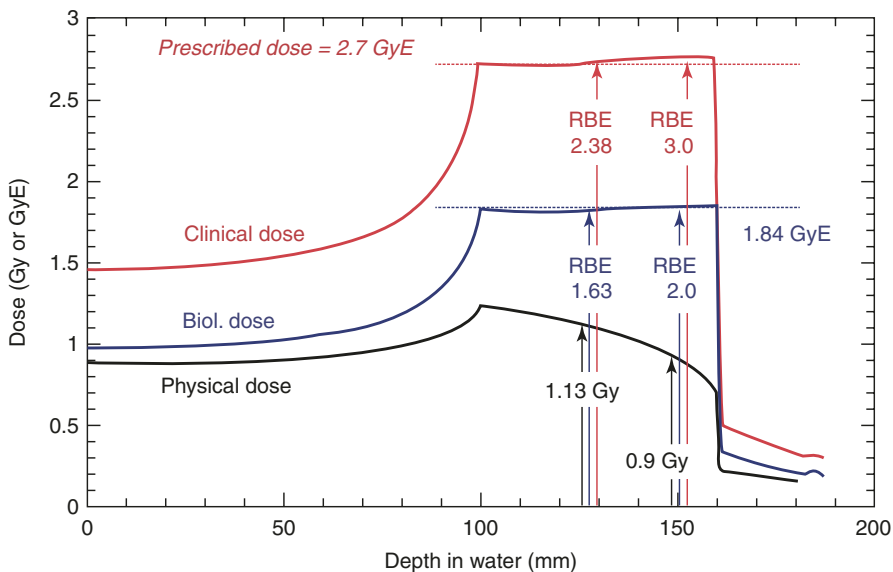

Fig. 1.7 Schematic method used to determine the RBE at the SOBP for the clinical situation (Reproducing the Figure with permission by the IAEA from International Atomic Energy Agency, MIZOE J. et al. "Clinical RBE determination scheme at NIRS-HIMAC," Relative Biological Effectiveness in Ion Beam Therapy, Technical Reports Series No. 461, IAEA, Vienna 135–152 [18])

– The GSI strategy is based on biophysical modeling [18]. The goal is to develop a model, which should be able to predict the response of the charged particle radiation from the known response of the biological object to photon radiation. This links the treatment planning for carbon therapy to the clinical experience with photon radiation. An example of such a model, the local effect model (LEM), has been implemented in treatment planning for carbon ion irradiation. The clinical results obtained at GSI are consistent with the predicted RBE values in that there is no significant clinical complication observed.

1.4   Range Uncertainty

The stopping power of an ion beam describes the energy loss of ions passing through matter per unit path length and determines the range of the ions and the ultimate depth of the Bragg peak. The stopping power is dependent on the energy of the ion beam and the atomic composition of the material. Uncertainty in the calculation of the stopping power then translates directly into uncertainty in the range and depth of the distal edge of the Bragg peak and in the dose distribution that is displayed by the treatment planning system.

All ion treatment planning is currently done using 3-D computed tomography (CT) images. The volumetric image consists of a 3-D voxel array of CT Hounsfield numbers (HU) that correspond to the attenuation coefficients of the material. To calculate the ion dose distribution, the HU must be converted to stopping power.

There are uncertainties in the HU to stopping power conversion that translate into significant uncertainties in the ion range and have a marked effect on the target margins that are used for treatment planning. Additionally, there are sources of uncertainty in HU resulting which are a function of patient size, CT scanner, scanning protocol, and reconstruction algorithm. In the HU to stopping power conversion, these uncertainties are combined with degeneracy in the mapping of HU to stopping power in the HU. Care must be taken in calibrating the CT scanner and HU to stopping power conversion to minimize the impact that this uncertainty has on target margins [20].

To ensure target coverage, despite these uncertainties, margins are added to the target during planning. The size of the margin is determined by the overall range uncertainty, which is typically proportional to 2.5–3.5% of the ion range with an additional 1.0–3.0 mm to account for range uncertainty that is not dependent on the dose calculation (e.g., setup error, measurement uncertainty, etc.) [21]. This margin is added to the distal and proximal extent of the target during treatment planning. Thus, the margin in the beam direction may be different from the lateral setup margin. The formula for calculating range uncertainty is as follows:

$$\text{Range Uncertainty}\left(\text{mm}\right) = \left(\text{Range}\left(\text{mm}\right) \times \text{Uncertainty}\left(\%\right)\right) + \text{Margin}\left(\text{mm}\right).$$

Figure 1.8 shows some common choices of uncertainty parameters and the significant effect that it has on the necessary target margins.
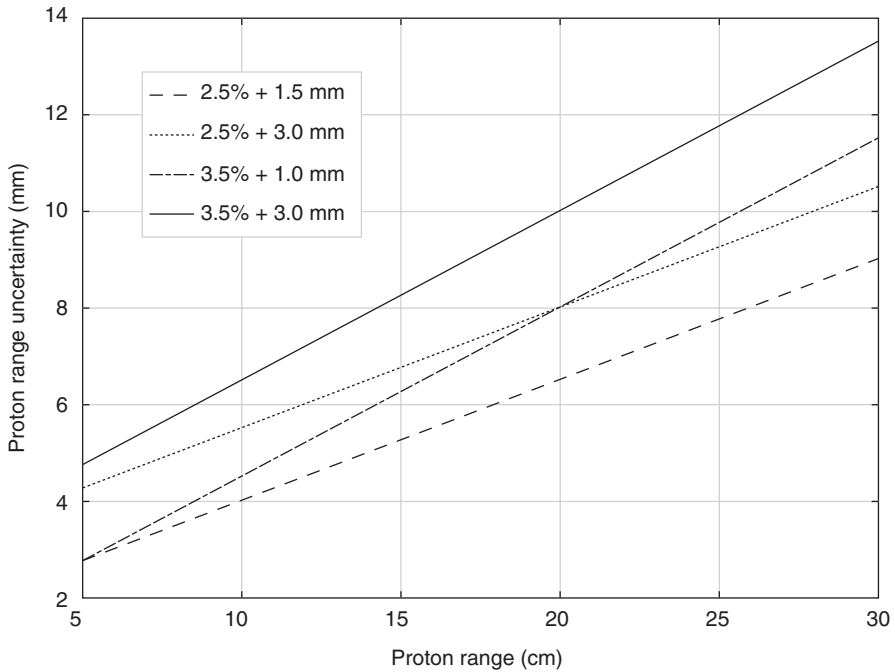
Fig. 1.8 Proton range uncertainty in millimeters plotted as a function of proton range in centimeters for various common choices of uncertainty parameters. The range uncertainty is calculated at the distal and proximal edges of the target and added to the target volume during planning (adapted from [21])

1.5   Beam Generators

- Clinically useable proton kinetic energies vary from ~70 to 250 MeV corresponding to 4 to 37 cm range in water. There are two types of accelerator systems used for proton therapy, a synchrotron and a cyclotron. In 2016, for ions heavier than protons, all accelerators were synchrotrons.

1.5.1   Synchrotron

- Figure 1.9 shows a photograph of a synchrotron.
- The synchrotron accelerates protons in a ring with a fixed radius orbit by boosting the proton's energy in each revolution in a fixed orbit.
- Low-energy particles are injected into the ring and are accelerated in an RF cavity placed within the ring. The generation of higher kinetic energy protons requires additional revolutions through the RF acceleration cavity. During each rotation the magnetic field that keep the protons constrained within the ring must be synchronously increased to maintain a stable proton orbit.
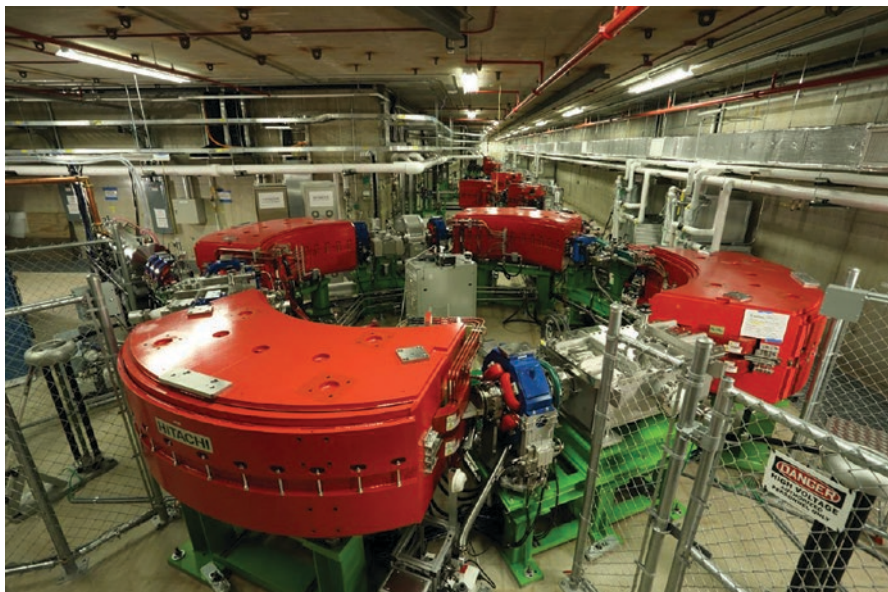
Fig. 1.9 Synchrotron at Mayo Clinic, Arizona. Photograph courtesy of Martin Bues

Once the protons are at the energy needed for treatment, they are "spilled" into the beam line and directed to the treatment room by a series of focusing and bending magnets. Synchrotrons produce beams in a pulsed beam structure requiring a period to "fill" for acceleration, then "spill" into the treatment rooms. This process typically takes 2–5 s per energy layer.

1.5.2 Cyclotron

Figure 1.10 shows a photograph of a cyclotron. A cyclotron accelerates protons within a fixed magnetic field. Low-energy protons are injected into the center of disk-shaped accelerating cavity. Particles gain kinetic energy by passing through RF accelerating cavities within the disk. The constant magnetic field binds the protons to a circular path within the disk, but, with each rotation, the protons that pass through the accelerating cavities gain energy and spiral radially outward incrementally increasing the energy. At the outer most orbit, the protons are "peeled" off and directed down the beam line for clinical use. All protons leaving the cyclotron are at the maximum clinically available energy. Since energies lower than the maximum are most commonly used, the proton beam is directed through low atomic number materials of variable thicknesses which interact with the protons to lower their energy to the required clinical energy. The cyclotron delivers a nearly continuous output of protons once the range and beam line magnets are set. Table 1.2 summarizes the differences between the two delivery systems.

Fig. 1.10 Cyclotron at ProCure Proton Therapy Center, NJ. Photograph courtesy of Dennis Mah

1.6 Future Developments

Light ion teletherapy is growing rapidly globally. Future developments are difficult to predict, but some developments include:

- Superconducting bending magnets and cyclotrons lead to more compact systems, but more complicated systems may have challenges with maintenance and downtime [22, 23].
- Range uncertainty is being addressed by a variety of different approaches including:
  - Proton CT—A proton beam is used like an x-ray to create a proton transmission CT image; the CT number to stopping power uncertainty is thus reduced. For some existing systems, this technique might be limited to thinner body sections because the maximum energy may not penetrate thick portions of the body. In addition, the energy/range relationship is dependent upon precise models of the proton trajectory [24].
  - Real-time diode dosimetry—A diode system is implanted into a body cavity, and the range is varied allowing the diode system to determine the range at which the protons can just be detected [25].
  - Prompt gamma imaging—Excited nuclei decay to the ground state emitting gamma rays up to 7 MeV. Knife edge slits collimate the gamma rays to within 2 mm. Initial results appear to be promising [26].

Table 1.2 Comparison of accelerator characteristics

	Magnetic field	Beam structure	Output energy
Synchrotron	Dynamic	Pulsed	Variable
Cyclotron	Constant	Continuous	Constant

- – Dual energy CT—Different energy CT scans are used to minimize uncertainties in CT numbers and provide additional information to convert CT numbers to stopping powers. The technique has not yet been proven to be sufficient over the range of compositions found in human body [27].
  - – PET imaging—Ions can generate short-lived positron-emitting isotopes which in turn produce annihilation photons which are detected by PET scanners. Biological and temporal wash out limit the utility [28].
  - – MRI—For craniospinal irradiation, the fatty replacement of vertebral bone is visible on MRI thereby illustrating where the beam stops [29]
- Interplay effects between the scanning beam and the internal motion of the patient may lead to hot and cold spots not represented in the plan. A variety of approaches are being actively studied including repainting, breath hold, abdominal compression, and robust optimization [30].
- Relative biological effectiveness—New calculation models are being studied to include the combined effects of LET and fractionation while simultaneously reducing calculation times [31]
  - – Further characterization of the clinical and biological effects of the enhanced RBE at the distal edge:
    - ∘ possible exploitation of end of range effects
    - ∘ Development of "biological dose painting" [32]

References

1. Blakely EA, Tobias CA, Ludewigt BA, Chu WT, Some physical and biological properties of light ions. In: Chu W, editor. Proceedings of the Fifth PTCOG Meeting & International Workshop on Biomedical Accelerators. Lawrence Berkeley Laboratories Report LBL-22962; 1986.
2. Chu WT, Ludewigt BA, Renner TR. Instrumentation for treatment of cancer using proton and light-ion beams. Lawrence Berkeley Laboratories Report LBL-33403, UC406; 1993.
3. Wambersie A, Deluca PM, Andreo P, Hendry JH. Light or heavy ions: a debate of terminology. Radiother Oncol. 2004;73(S2):iiii.
4. Vatnitsky SM, Moyers MF. Radiation therapy with light ions. In: van Dyk J, editor. The modern technology of radiation oncology v.3: A compendium for medical physicists and radiation oncologists. Wisconsin: Medical Physics Publishing; 2013. p. 183–222. ISBN: 978-1-930524-57-6.
5. Jermann M. Particle therapy statistics in 2014. Int J of Particle Therapy. 2015;2(1):50–4.
6. Goitein M. Radiation oncology: A Physicist's-eye. New York: Springer-Verlag; 2008.
7. Moyers MF, Stanislav V. Practical implementation of light ion beam treatments. Madison, WI: Medical Physics Publishing; 2012.
8. Metcalfe P, Kron T, Hoban P. The physics of radiotherapy X-rays from linear accelerators. Madison, WI: Medical Physics Publishing; 2007.
9. Dowdell SJ, Clasie B, Depauw N, Metcalfe P, Rosenfeld AB, Kooy HM, Flanz JB, Paganetti H. Monte Carlo study of the potential reduction in out-of-field dose using a patient-specific aperture in pencil beam scanning proton therapy. Phys Med Biol. 2012;57:2829–42.

10. Moteabbed M, Yock TI, Depauw N, Madden TM, Kooy HM, Paganetti H. Impact of spot size and beam-shaping devices on the treatment plan quality for pencil beam scanning proton therapy. Int J Radiat Oncol Biol Phys. 2016;95:190–8.
11. Paganetti H, editor. Proton therapy physics. Boca Raton, FL: CRC Press; 2011.
12. Paganetti H, Jiang H, Parodi K, Slopsema R, Engelsman M. Clinical implementation of full Monte Carlo dose calculation in proton beam therapy. Phys Med Biol. 2008;53:4825–53.
13. Paganetti H. Relating proton treatments to photon treatments via the relative biological effectiveness-should we revise current clinical practice? Int J Radiat Oncol Biol Phys. 2015;91:892–4.
14. Paganetti H. Relative biological effectiveness (RBE) values for proton beam therapy. Variations as a function of biological endpoint, dose, and linear energy transfer. Phys Med Biol. 2014;59:R419–72.
15. Cuaron JJ, Chang C, Lovelock M, et al. Exponential increase in relative biological effectiveness along distal edge of a proton Bragg peak as measured by deoxyribonucleic acid double-strand breaks. Int J Radiat Oncol Biol Phys. 2016;95:62–9.
16. ICRU. Prescribing, recording, and reporting proton-beam therapy. J ICRU. 2007;78:7.
17. Grassberger C, Trofimov A, Lomax A, et al. Variations in linear energy transfer within clinical proton therapy fields and the potential for biological treatment planning. Int J Radiat Oncol Biol Phys. 2011;80:1559–66.
18. Relative biological effectiveness in ion beam therapy. IAEA Technical Reports Series. 2008;461:1–165.
19. De Laney TF, Kooy HM. Proton and charged particle radiotherapy. Philadelphia: Lippincott Williams & Wilkins; 2008.
20. Ainsley CG, Yeager CM. Practical considerations in the calibration of CT scanners for proton therapy. J Appl Clin Med Phys. 2014;15(3):4721.
21. Paganetti H. Range uncertainties in proton therapy and the role of Monte Carlo simulations. Phys Med Biol. 2012;57(11):R99–117.
22. Blosser HG. Compact superconducting synchrocyclotron systems for proton therapy. Nucl Inst Methods Phys Res Sec B. 1989;40–41:1326–30.
23. Robin DS, Arbelaez D, Caspi S, Sun C, Sessler A, Wan W, Yoon M. Superconducting toroidal combined-function magnet for a compact ion beam cancer therapy gantry. Nucl Instrum Methods Phys Res A. 2011;659(1):484–93.
24. Schneider U, Pedroni E. Proton radiography as a tool for quality control in proton therapy. Med Phys. 1995;22:353–63.
25. Tang S, Both S, Bentefour EH, Paly JJ, Tochner Z, Efstathiou J, Lu HM. Improvement of prostate treatment by anterior proton fields. Int J Radiat Oncol Biol Phys. 2012;83:408–18.
26. Richter C, Pausch G, Barczyk S, Priegnitz M, Keitz I, Thiele J, Smeets J, et al. First clinical application of a prompt gamma based in vivo proton range verification system. Radiother Oncol. 2016; 118:232–7.
27. Yang M, Virshup G, Clayton J, Zhu XR, Mohan R, Dong L. Does kV-MV dual-energy computed tomography have an advantage in determining proton stopping power ratios in patients? Phys Med Biol. 2011;56:4499–515.
28. Knopf A, Parodi K, Bortfeld T, Shih HA, Paganetti H. Systematic analysis of biological and physical limitations of proton beam range verification with offline PET/CT scans. Phys Med Biol. 2009;54:4477–95.
29. Krejcarek SC, Grant PE, Henson JW, Tarbell NJ, Yock TI. Physiologic and radiographic evidence of the distal edge of the proton beam in craniospinal irradiation. Int J Radiat Oncol Biol Phys. 2007;68:646–9.
30. Rietzel E, Bert C. Respiratory motion management in particle therapy. Med Phys. 2010;37:449–60.
31. Wedenberg M, Lind BK, Hårdemark B. A model for the relative biological effectiveness of protons: the tissue specific parameter α/β of photons is a predictor of the sensitivity to LET changes. Acta Oncol. 2013;52:580–8.
32. Ling CC, Humm J, Larson S, Amols H, Fuks Z, Leibel S, Koutcher JA. Towards multidimensional radiotherapy (MD-CRT): biological imaging and biological conformality. Int J Radiat Oncol Biol Phys. 2000;47:551–60.